catalysts

MDPI

Article

Catalytic Performance of Bimetallic Systems (Cu-Fe, Cu-Mn, Fe-Mn) Based on Spherical MCM-41 Modified by Template Ion-Exchange in NH_3-SCR Process

Aleksandra Jankowska [1], Andrzej Kowalczyk [1], Małgorzata Rutkowska [1], Marek Michalik [2] and Lucjan Chmielarz [1,*]

[1] Faculty of Chemistry, Jagiellonian University, Gronostajowa 2, 30-387 Kraków, Poland
[2] Institute of Geological Sciences, Jagiellonian University, Gronostajowa 3a, 30-387 Kraków, Poland
* Correspondence: chmielar@chemia.uj.edu.pl; Tel.: +48-12-686-24-17

Abstract: Mesoporous silica of MCM-41 type with spherical morphology was modified with copper, iron, or manganese as well as pairs of these metals by template ion-exchange (TIE) method. The obtained samples were characterized with respect to their structure (XRD), morphology (SEM-EDS), textural parameters (low-temperature N_2 sorption), surface acidity (NH_3-TPD), transition metal loadings (ICP-OES), their deposited forms (UV-vis DRS) and reducibility (H_2-TPR). The catalytic performance of monometallic and bimetallic samples in the selective catalytic reduction of NO with ammonia (NH_3-SCR) was tested. The best catalytic results presented a bimetallic copper-manganese sample, which was significantly more active than the mechanical mixture of monometallic copper and manganese catalysts. The synergistic cooperation of manganese and copper species is possibly related to charge relocation between them, resulting in activation of the catalyst in oxidation of NO to NO_2, which is necessary for the fast NH_3-SCR reaction.

Keywords: NH_3-SCR; spherical MCM-41; copper; iron; manganese; template ion-exchange method

Citation: Jankowska, A.; Kowalczyk, A.; Rutkowska, M.; Michalik, M.; Chmielarz, L. Catalytic Performance of Bimetallic Systems (Cu-Fe, Cu-Mn, Fe-Mn) Based on Spherical MCM-41 Modified by Template Ion-Exchange in NH_3-SCR Process. *Catalysts* **2022**, *12*, 885. https://doi.org/10.3390/catal12080885

Academic Editor: Rufino M. Navarro Yerga

Received: 14 July 2022
Accepted: 10 August 2022
Published: 12 August 2022

1. Introduction

Selective catalytic reduction of nitrogen oxides (NO_x, where x is 1 or 2) using NH_3 as the reducing agent (NH_3-SCR) was patented by the Engelhard Corporation (USA) in 1957 [1]. The first large-scale NH_3-SCR installation was implemented by the IHI Corporation in 1978 [2]. Nowadays, NH_3-SCR technology is used in the most important commercial methods used for the control of NO_x emissions by electric power stations as well as waste treatment plants [3]. Monolithic vanadium-based catalysts, such as V_2O_5-WO_3/TiO_2 or V_2O_5-MoO_3/TiO_2, are typically used as industrial NH_3-SCR catalysts for the conversion of NO_x emitted from such stationary sources [4]. In recent decades, the NH_3-SCR process has been adapted for NO_x conversion in exhaust gases of diesel vehicles [5]. This technology, called Blue Tec, utilises aqueous urea solution, which is hydrolysed to NH_3 and CO_2 before ammonia is used as a reducing agent for NO_x conversion, similar to a typical NH_3-SCR process. Cu-exchanged zeolites, such as Cu-CHA, are used as catalysts in urea-based SCR systems in diesel vehicles [6]. In general, NH_3-SCR technology is a mature and well-optimised method utilised for NO_x emission control in electric power stations and industrial boilers. However, there are some drawbacks to this technology that limit its adaptation to current needs. The most important is related to the operation of the NH_3-SCR monolithic converters with dusty gases, which may result in clogging of channels and finally decrease the efficiency of the NO_x conversion. Nowadays, most of the NH_3-SCR converters are located upstream of an electrostatic precipitator (ESP) and therefore operate with a dusty gas stream (high-dust NH_3-SCR). To solve the monolith clogging problem, flue gases de-dusting in the ESP unit should be undertaken prior to the exhaust gas being directed to the NH_3-SCR converter (low-dust NH_3-SCR). The problem is that the ESP units

effectively operate only with relatively cold flue gases, at 250 °C or even lower. Thus, in such modified installations that operate with commercial vanadium-based catalysts of the NH_3-SCR process, the de-dusted gas, downstream of the ESP unit, must be additionally heated to above 300 °C prior to being directed to the NH_3-SCR converter [4,7]. Of course, such rearrangement of the exhaust gas purification system should result in protection of the monolithic catalysts against clogging by dust particles; however, it increases the operating costs of such an installation due to the additional heating of the exhaust gases downstream of the ESP unit. An optional, possibly cheaper, solution could be an effective NO_x conversion at a temperature below 250 °C without the need to heat the exhaust gases between the ESP and NH_3-SCR units. However, to implement this option, the development of an effective catalyst of the NH_3-SCR process operating at temperatures below 250 °C is necessary.

Mesoporous silica materials are very promising supports of low-temperature NH_3-SCR catalysts [4,8–10]. Such materials, produced by the surfactant directed methods, are characterized by uniform mesoporous structure, high surface area and thermal and hydrothermal stability in the temperature range of the low-temperature NH_3-SCR process. Catalytically active components can be effectively deposited on the silica surface in highly dispersed form by the template ion-exchange (TIE) method [4,8–11]. Our previous studies of MCM-41 modified with copper and iron showed its very promising catalytic performance in the NH_3-SCR process [4,8–10]. Copper modified silica, especially by the TIE method, presented a very good catalytic activity in the low-temperature range [4,8–10], while the iron-doped mesoporous silica samples were catalytically active at higher temperatures [4,8–10]. Moreover, our previous studies [4,9] showed that deposition of copper and iron on spherical MCM-41 resulted in the catalysts being more selective to nitrogen and effectively operating in a slightly broader temperature range comparing to the analogous catalysts based on cylindrical MCM-41. This is possibly related to the shorter residence time of reactant molecules inside pores of MCM-41 and therefore also lower risk of the side reactions (e.g., NH_3 to NO oxidation). An important additional conclusion is related to the incorporation of aluminium into silica walls prior to transition metals deposition. It has been shown that the generation of acid sites by aluminium species incorporated into MCM-41 walls is not beneficial for the low-temperature NH_3-SCR process, but results in activation of the catalysts at higher temperatures [12]. Manganese is another component of the low-temperature NH_3-SCR catalysts broadly reported in the scientific literature [13–15]. Manganese may exist in different oxidations states, such as Mn^{2+}, Mn^{3+} and Mn^{4+}, however it has been postulated that Mn^{4+} is the most active in the low-temperature NH_3-SCR process [16], because it can promote NO oxidation to NO_2, which is necessary for the fast NH_3-SCR reaction ($2NH_3 + NO + NO_2 \rightarrow 2N_2 + 3H_2O$) [17]. On the other hand, such a high activity of manganese in oxidation processes is possibly responsible for direct ammonia oxidation at higher temperatures and therefore a decrease in the NH_3-SCR efficiency in this range [18].

The main goal of the studies was the determination of the catalytic performance of transition metal pairs (Cu-Fe, Cu-Mn, and Fe-Mn) deposited on spherical MCM-41 by TIE method as well as analysis of the possible synergistic interactions between these metals in the NH_3-SCR process. High surface area mesoporous silica materials as well as application of TIE method for metal deposition should result in catalysts with a high contribution of surface available catalytically active monometallic and bimetallic species. This is a very important advantage of this type of catalyst in comparison with unsupported mixed metal oxide catalysts. Moreover, the relatively wide channels (in mesoporous range) should ensure effective reactant diffusion. Thus, such catalytic systems offer some advantages for the effective catalyst design.

2. Results and Discussion

The spherical morphology of MCM-41 was proved by scanning electron microscopy (SEM). The size of the silica spheres was in the range of 600–700 nm with a smaller contribution of spheres with diameters below 300 nm (Supplementary Materials, Figure S1). Deposi-

tion of transition metals into S-MCM-41 (monometallic and bimetallic samples) did not result in significant changes in silica morphology (Supplementary Materials, Figures S2 and S3). However, as verified by EDS analysis, nanorods of CuO were identified in the CuFe sample. The thickness of such nanorods was about 50–60 nm, while their length was typically above 3000 nm. Moreover, in the case of this sample, small aggregates of CuO with an average diameter of 30–50 nm, deposited on the surface of silica spheres, could be identified (Supplementary Materials, Figure S3A). The formation of similar CuO nanorods has been reported for copper oxide synthesized by wet chemical-assisted hydrothermal processing using polyethylene glycol (PEG 4000) as the structure-directing template [19]. On the other hand, the formation of similar nanorod Fe_2O_3 crystallites has been reported in our previous studies [11,20] for iron deposition into as-prepared MCM-41 by the TIE method. Hexadecyltrimethylammonium cations extracted from pores of as-prepared S-MCM-41 to the solution of $CuCl_2$ can possibly play a role of structure-directing agent, similar to PEG 4000 [19]. This interesting effect needs additional studies to explain the mechanism behind such nanorod metal oxides formation.

The XRD patterns of spherical MCM-41 (S-MCM-41) and its modifications with transition metals—Cu, Fe and Mn—deposited by the TIE method are shown in Figure 1(A1,A2). In diffractogram of S-MCM-41 three reflections, (100), (110) and (200), characteristic of the hexagonal structure of MCM-41, are observed. Deposition of transition metals only slightly decreased the intensity of these diffraction peaks (Figure 1(A1)) indicating that the TIE method did not result in a significant destruction of the ordered porous structure of S-MCM-41. On the other hand, a shift of (100) diffraction peak into higher values of 2θ (Figure 1(A1)) is possibly related to the deposition of transition metal species inside pores and therefore decreasing their size. In the case of S-MCM-41 modified with copper species, the sample Cu, reflections characteristic of small CuO crystallites were found (Figure 1(A2)). The estimated size of CuO crystallites (about 30 nm) is significantly larger than the pore diameter of S-MCM-41 (3.25 nm), indicating that copper oxide crystallites are located outside of the mesoporous system of the silica support. Similar reflections, characteristic of iron and manganese oxides were not found in the S-MCM-41 samples modified with these transition metals. Deposition of transition metal pairs by the TIE method significantly decreased the intensity of the (100), (110) and (200) diffraction peaks (Figure 1(B1)), indicating partial destruction of the ordered porous structure of S-MCM-41. This effect is the most significant for the FeMn sample. Deposition of transition metal pairs, similar to the monometallic samples, shifted the (100) reflection into slightly higher values of 2θ, indicating a possible decrease in pore size due to deposition of metal species inside pores. In the case of the CuFe sample, the low-intensive reflections characteristic of CuO can be identified (Figure 1(B2)). Such diffraction peaks are not present in the diffraction pattern of the CuMn sample. Thus, deposition of manganese together with copper inhibits aggregation of copper species into CuO crystallites.

The nitrogen adsorption–desorption isotherms of S-MCM-41 and its modifications with manganese, iron, and copper, presented in Figure S4A (Supplementary Materials), are classified as type IV according to the IUPAC standards and are characteristic of mesoporous materials, such as MCM-41 [21,22]. The characteristic feature of the recorded isotherms is a steep increase in nitrogen uptake at relative pressure of 0.15–0.30 assigned to the capillary condensation of N_2 molecules inside mesopores. Deposition of transition metal pairs resulted in a small decrease in nitrogen uptake, indicating a decrease of mesopore volume, possibly related to deposition of the larger amount of transition metal species deposited inside mesopores (Supplementary Materials, Figure S4B). An additional increase in nitrogen sorption, observed for the CuMn sample in the relative pressure range of 0.5–0.9, is possibly related to the presence of larger pores located between sticked silica spheres. The hysteresis loops in adsorption–desorption isotherms belong to the H3 category according to the IUPAC classification characteristic of the pore network consisting of large pores only partially filled with the condensate [21,22].

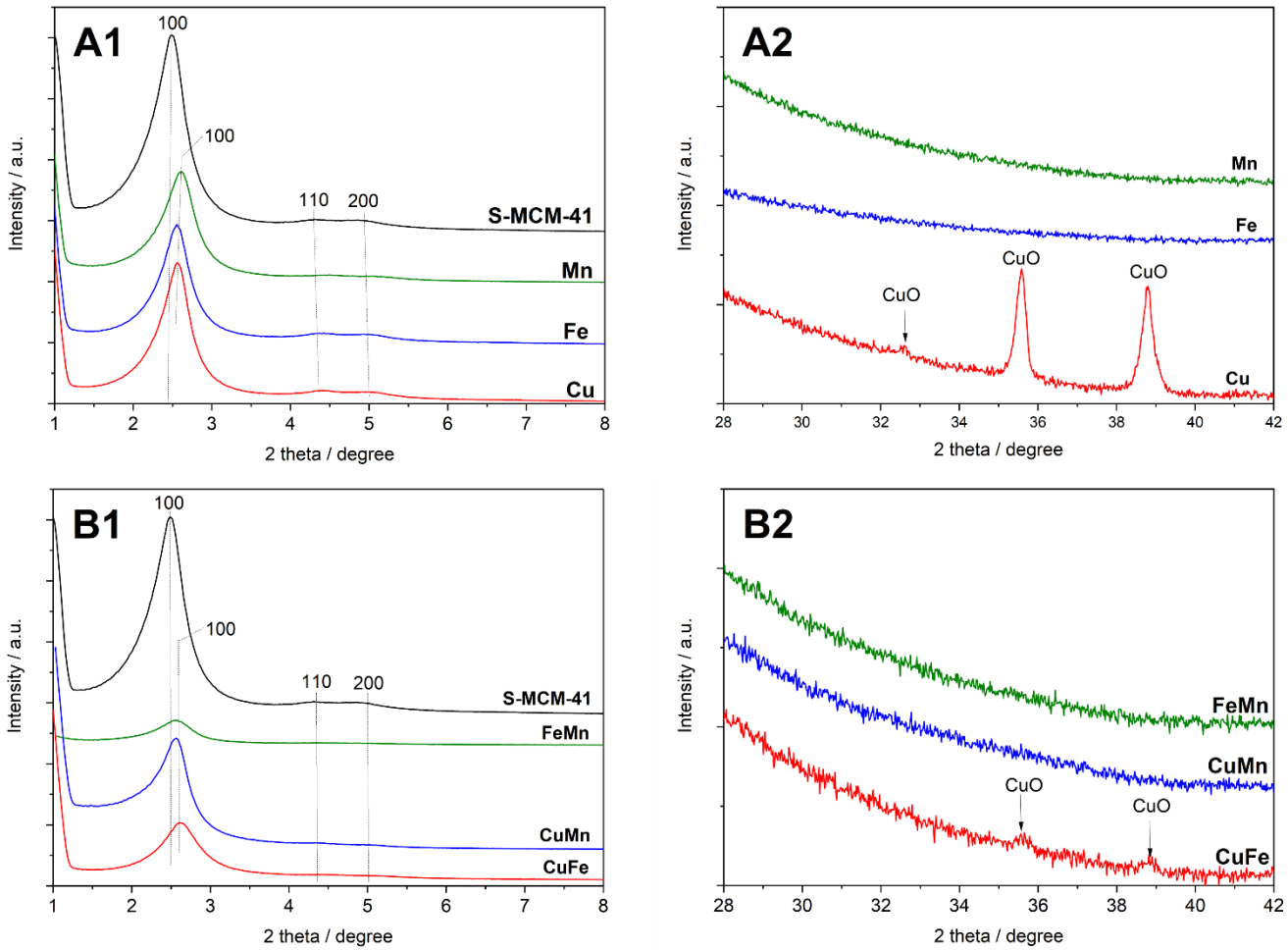

Figure 1. Powder XRD diffractograms of the spherical MCM-41 samples modified by TIE method with Cu, Fe, Mn ((**A1**)—low angle range, (**A2**)—high angle range) and their bimetallic systems ((**B1**)—low angle range, (**B2**)—high angle range).

The profiles of pore size distribution (PSD) determined for S-MCM-41 and its modifications are presented in Figure 2. The PSD profile of S-MCM-41 shows its uniform porous structure with the maximum pore diameter at about 3.3 nm. Deposition of transition metals resulted in a decrease of PSD maximum intensity and shift of the maximum to lower diameters (3.1–3.2 nm), indicating deposition of transition metal species inside pores (Figure 2A). This effect was more significant for the samples modified with transition metal pairs (Figure 2B). In this case pore diameter decreased to about 3.0–3.2 nm.

Textural parameters of the samples are compared in Table 1. The specific surface area (S_{BET}) determined for S-MCM-41 is 1063 $m^2 \cdot g^{-1}$. Deposition of transition metals decreased S_{BET} by less than 3% and pore volume by less than 18%. In the case of the samples modified with pairs of transition metals, the S_{BET} values decreased by 2–16% and pore volume by about 12–19%.

The content of transition metals deposited to S-MCM-41 is presented in Table 1. In the case of the monometallic samples, the metal loading is in the range of 1.4–1.9 wt%, while for the bimetallic samples the loading of each deposited transition metal is in the range of 1.3–1.9 wt%.

The coordination and aggregation of transition metals introduced into S-MCM-41 were analysed by UV-vis DR spectroscopy. Figure 3 presents the spectra recorded for the monometallic samples. The spectrum of the Cu sample contains main maximum at about 230 nm assigned to monomeric Cu^{2+} ions interacting with oxygens of silica ($O^{2-} \rightarrow Cu^{2+}$) [23,24]. The presence of monomeric Cu^{2+} ions is also proved by the presence

of the band at about 650 nm related to d-d transition of Cu^{2+} ions in pseudo-octahedral coordination (e.g., $Cu(H_2O)_6^{2+}$) [23,24]. The increased level of absorbance, observed above 300 nm, is assigned to the aggregated copper oxide species of different sizes (oligomeric and small crystallites) [24,25].

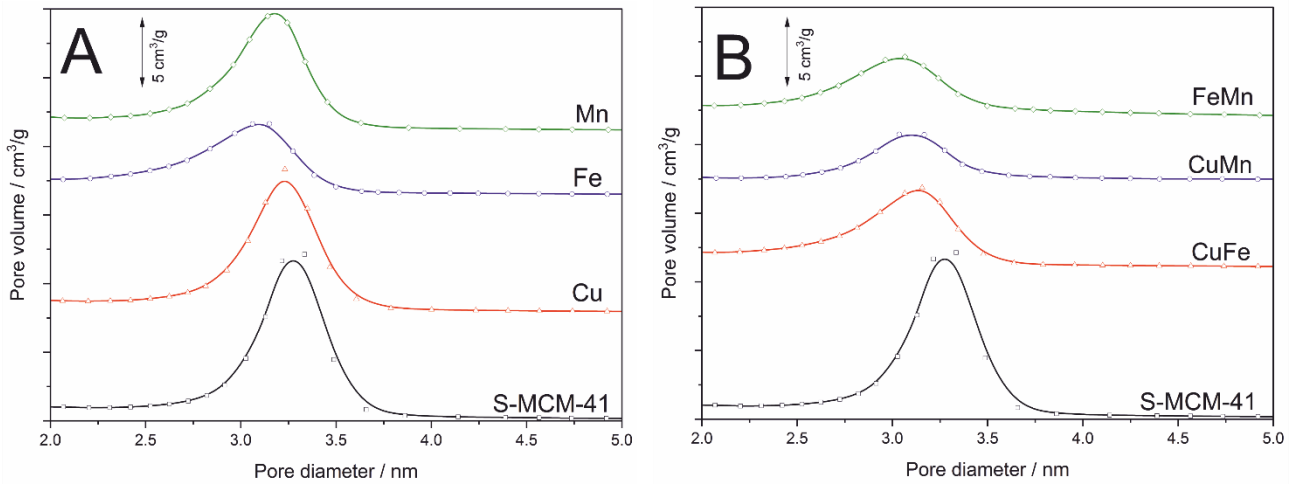

Figure 2. Pore size distributions of the spherical MCM-41 samples modified by TIE method with Cu, Fe, Mn (**A**) and their bimetallic systems (**B**).

Table 1. Textural parameters, chemical composition and surface acidity of transition metals modified S-MCM-41 samples.

Sample Code	S_{BET}/ $m^2 \cdot g^{-1}$	Pore Volume/ $cm^3 \cdot g^{-1}$	Pore Diameter/ nm	Cu/ wt%	Fe/ wt%	Mn/ wt%	[1] C_a/ $\mu mol \cdot g^{-1}$	[2] D_a/ $\mu mol \cdot m^{-2}$
S-MCM-41	1063	0.90	3.3	-	-	-	-	-
Cu	1035	0.74	3.2	1.9	-	-	57	0.055
Fe	1035	0.75	3.1	-	1.6	-	108	0.104
Mn	1061	0.88	3.2	-	-	1.4	93	0.088
CuFe	1047	0.75	3.2	1.9	1.6	-	207	0.198
CuMn	889	0.79	3.1	1.9	-	1.4	144	0.162
FeMn	947	0.73	3.0	-	1.7	1.3	212	0.224

[1] Surface concentration of acid sites related to 1 g of the sample. [2] Surface density of acid sites—concentration of acid sites on 1 m^2 of the sample.

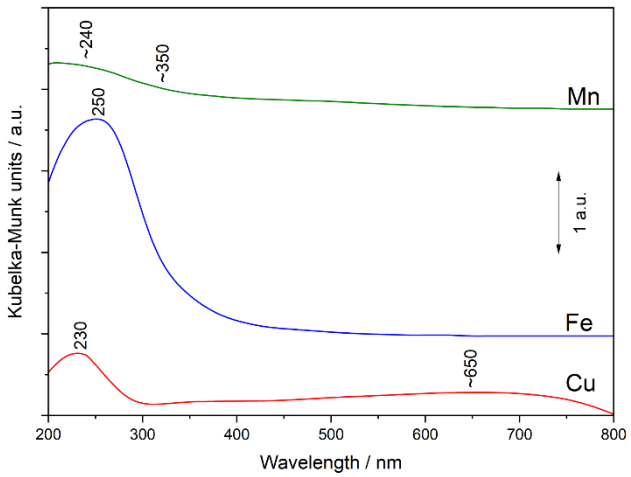

Figure 3. UV-vis DR spectra of the spherical MCM-41 samples by TIE method with Cu, Fe and Mn.

The main band in the spectrum of the Fe sample (Figure 3), located at about 250 nm, is possibly a superposition of three bands. The band assigned to monomeric Fe^{3+} cations in tetrahedral coordination is expected at about 210 nm. The band related to mononuclear Fe^{3+} ions in octahedral coordination, which possibly dominate in the studied sample, should appear at about 260 nm [25–27]. The shoulder at about 300–400 nm is characteristic of small oligonuclear Fe_xO_y clusters [28]. Thus, the obtained results indicate that Fe^{2+} was oxidised to Fe^{3+} during iron deposition process, possibly in calcination step. Iron was deposited in the form of highly dispersed species, mainly as mononuclear Fe^{3+} ions in octahedral coordination, which is in line with the results of XRD studies (Figure 1(A2)).

The broad band, located in a spectrum of the Mn sample below 350 nm, is possibly a superposition of two sub-bands. The first, expected at about 240 nm, is assigned to the O-Mn^{2+} ligand-to-metal charge-transfer transition and the $^6A_{1g} \rightarrow {}^4T_{1g}$ ligand field transition of distorted octahedral Mn^{2+}. The band at 315 nm is related to O-Mn^{3+} ligand-to-metal charge-transfer transition [29]. Moreover, the broad shoulder above 350 nm is possibly related to the O-Mn^{2+} ligand-to-metal $^6A_{1g} \rightarrow {}^4T_{2g}$ transition [29]. Thus, the obtained results indicate that part of Mn^{2+} cations were oxidized to Mn^{3+} ions.

An analysis of UV-vis DR spectra of the bimetallic samples is difficult due to overlapping bands originated from different metal species. To identify the differences in the forms of metal species in the bimetallic and monometallic samples, the original spectra of the bimetallic samples were compared to the sum of the monometallic samples' spectra (Figure 4). The main difference in the spectrum of the bimetallic CuFe sample and the sum of the monometallic samples' spectra (Cu+Fe) is related to the increased level of absorbance observed above 450 nm (Figure 4A) assigned to the presence of aggregated copper oxide species in the Cu sample [24,25]. Thus, the UV-vis DRS studies proved the results of XRD studies (Figure 1(A2,B2)), showing that deposition of copper and iron significantly limits the formation of CuO crystallites.

The spectrum of the bimetallic CuMn sample consists of the asymmetric band centred at about 225 nm, related to monomeric Cu^{2+} and Mn^{2+} cations (Figure 4B). In the case of the cumulative spectrum of the monomeric samples (Cu+Mn), this band is located exactly in the same position. The shoulder above 400 nm in a spectrum of the CuMn sample is possibly related to the presence of Mn^{2+} cations [29]. However, this shoulder could also be assigned to the presence of aggregated, possibly oligomeric, copper oxide species [24,25]. The increased level of absorbance at higher wavelength, characteristic of the presence of CuO aggregates, is less intensive in the spectrum of the CuMn sample comparing to the sum of the Cu and Mn spectra (Cu+Mn), indicating limited contribution of such aggregates in the bimetallic sample.

The spectrum of the FeMn sample consists of the band centred at about 240 nm and the shoulder above 340 nm (Figure 4C). The main peak is related to monomeric Fe^{3+} and Mn^{2+} cations, while the shoulder is assigned to oligomeric iron oxide species (region about 340 nm), Mn^{3+} cations (region about 340 nm) and Mn^{2+} (region above 450 nm) [25–27,29]. The cumulative spectrum of the Fe and Mn samples (Fe+Mn) is very similar to the spectrum of the bimetallic FeMn sample.

Reducibility of transition metal species deposited on S-MCM-41 was analysed by a temperature-programmed reduction method (H_2-TPR). The reduction profile of the Cu sample consists of a sharp peak at about 260 °C with a shoulder at 215 °C and a broad peak at about 510 °C (Figure 5). The low-temperature shoulder at about 215 °C is possibly assigned to the reduction of copper ($Cu^{2+} \rightarrow Cu^0$) in the form of oligomeric copper oxide species and CuO crystallites [30]. The peak at 260 °C is related to the reduction of monomeric Cu^{2+} cations to Cu^+ species, while the broad maximum of about 510 °C is a possible superposition representing two processes—reduction of monomeric Cu^+ cations to Cu^0 [31] expected below 450 °C as well as reduction of strongly stabilized copper species (possibly at higher temperatures). Thus, the results of H_2-TPR prove that copper was deposited into S-MCM-41 in the form of monomeric cations together with aggregated metal oxide species.

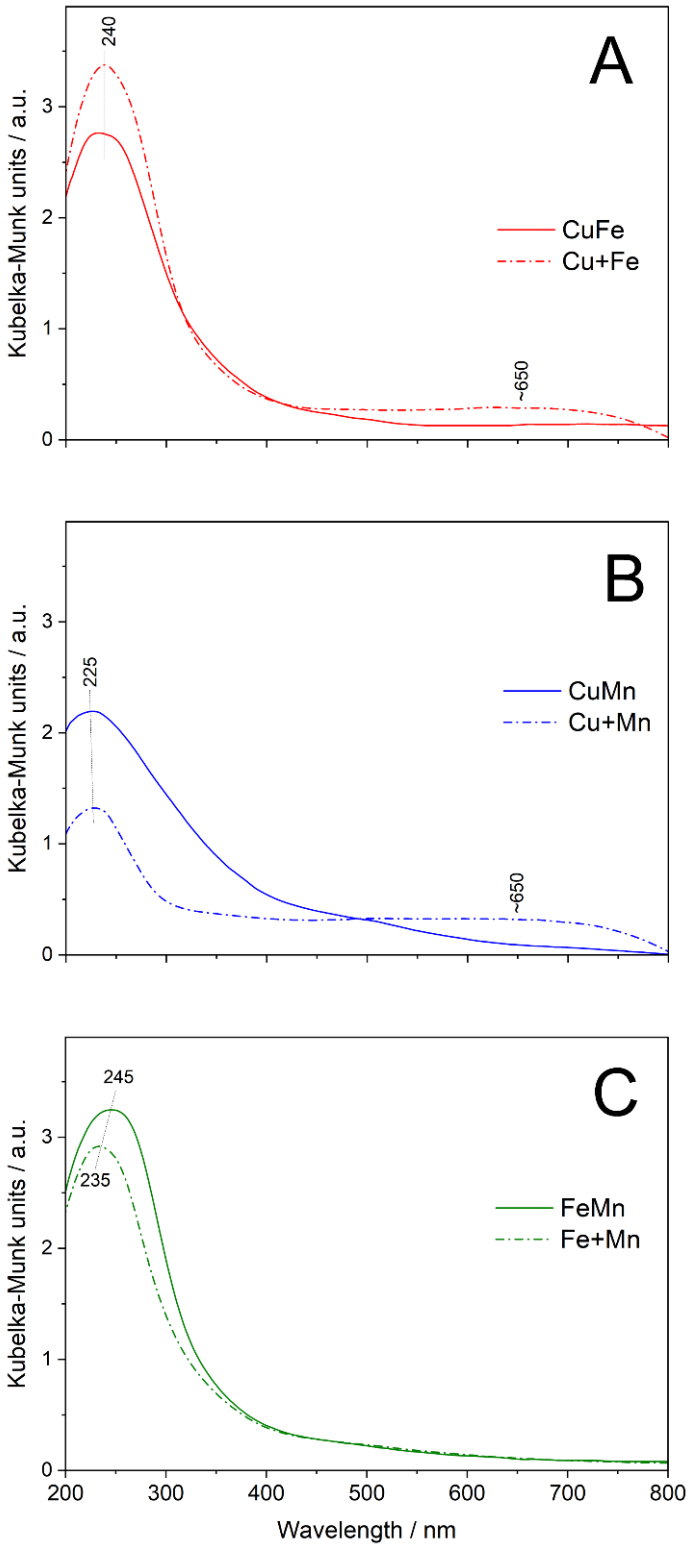

Figure 4. UV-vis DR spectra of spherical MCM-41modified with CuFe (**A**), CuMn (**B**), and FeMn (**C**) bimetallic system and for comparison sums of the spectra of monometallic samples Cu+Fe (**A**), Cu+Mn (**B**) and Fe+Mn (**C**) marked by dash-dot lines.

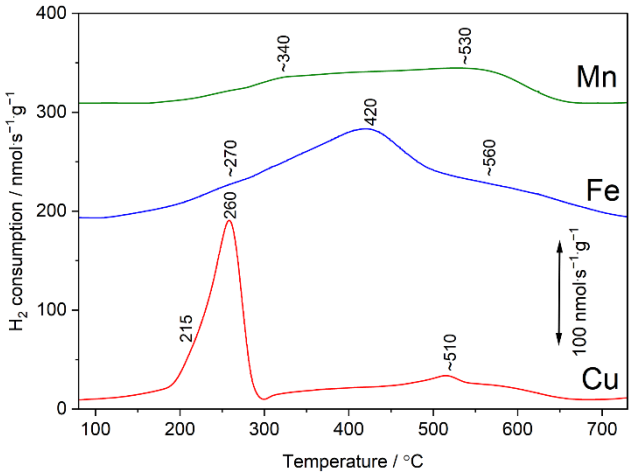

Figure 5. Results of H_2-TPR studies of the spherical MCM-41 based samples modified with Cu, Fe and Mn by TIE method.

Reduction profile of the Fe sample consists of a broad peak spread in the range of 120–725 °C with the main maximum at about 420 °C and two shoulders at 270 and 560 °C (Figure 5). It has been reported that reduction ($Fe^{3+} \rightarrow Fe^{2+}$) temperature of iron species deposited on mesoporous silicas decreases with an increase in their aggregation [32–34]. Therefore, it seems that the low-temperature peak at 270 °C is assigned to the reduction of Fe^{3+} to Fe^{2+} cations in aggregated metal oxide species, while the main maximum at 420 °C is related to the reduction of monomeric Fe^{3+} cations to Fe^{2+}. The broad maximum at about 560 °C is related to the reduction of Fe^{2+} to Fe^0 [35]. Thus, iron deposited into S-MCM-41 is present mainly in the form of monomeric cations with the smaller contribution of aggregated metal oxide species.

The reduction profile of the Mn sample is spread in the range of 170–660 °C and consists of at least two overlapping peaks at about 340 and 530 °C (Figure 5). The low-temperature peak is assigned to the reduction of highly dispersed Mn_3O_4 species to MnO, while the high-temperature maximum is possibly attributed to the reduction of more aggregated Mn_3O_4 species [36,37].

The analysis of H_2-TPR profiles of the bimetallic samples is difficult due to the overlapping of the reduction peaks originating from different metal species. Therefore, the reduction profiles of the bimetallic samples were compared with the cumulative profiles of the monometallic samples (Figure 6). The reduction profile of the CuFe sample consists of three low-temperature peaks at 190, 235 and 300 °C and a broad high-temperature maximum at about 560 °C (Figure 6A). The peak at 190 °C is possibly related to the reduction of copper ($Cu^{2+} \rightarrow Cu^0$) in the form of oligomeric copper oxide species and small CuO crystallites [30], while the maxima at 235 and 300 °C are assigned to two overlapping processes—reduction of monomeric Cu^{2+} cations to Cu^+ [31] as well as reduction of Fe^{3+} to Fe^{2+} cations in iron oxide species [33,34]. The broad high-temperature shoulder above 350 °C is related to the reduction of monomeric Cu^+ cations to Cu^0 [31], while at higher temperatures (peak at 560 °C) reduction of Fe^{2+} to Fe^0 is observed [35]. However, the reduction of strongly stabilized copper species at higher temperatures cannot be excluded. There are significant differences in the profiles of the bimetallic CuFe sample and cumulative profile of the monometallic (Cu+Fe) samples (Figure 6A), indicating the formation of easy-reducible copper species (reduction below 200 °C) as well as the higher contribution of monomeric copper cations in the CuFe sample than in the Cu sample. These results are in line with the conclusions of the XRD (Figure 1(A2)) and UV-vis DRS studies (Figure 4A).

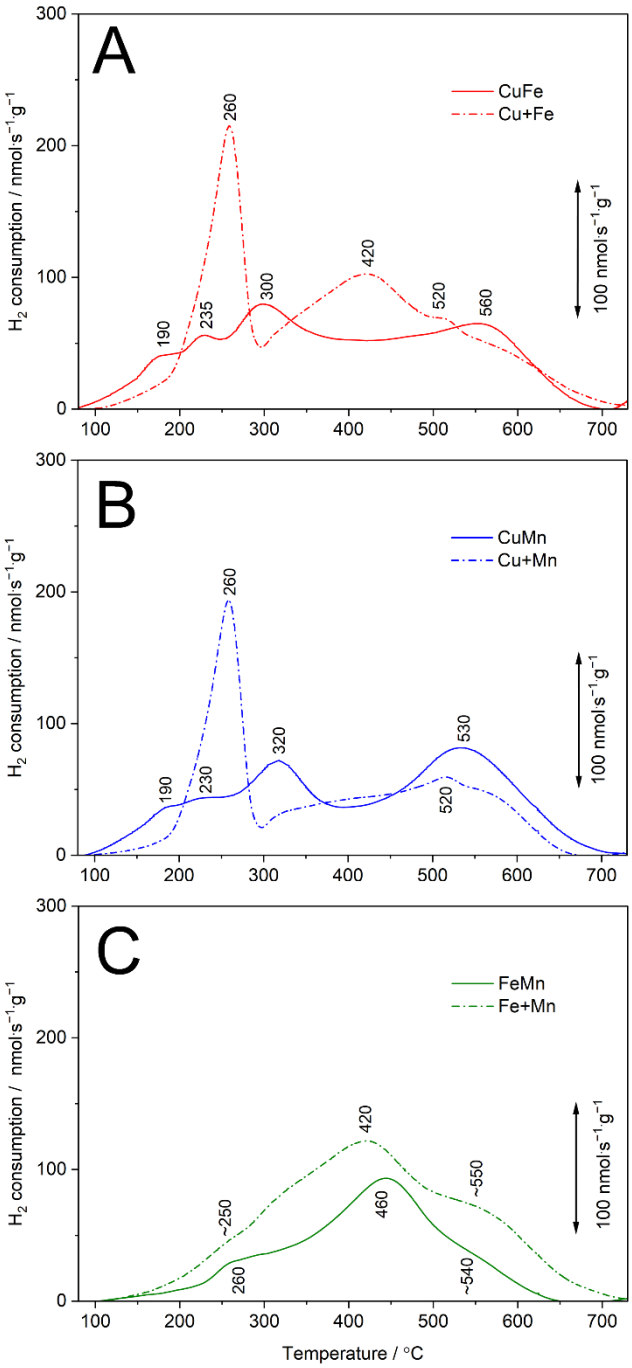

Figure 6. Results of H_2-TPR studies of the spherical MCM-41 samples modified by TIE method with CuFe (**A**), CuMn (**B**) and FeMn (**C**) bimetallic system and reduction profiles of the monometallic combined samples (dash-dot line).

The reduction profile of the CuMn sample consists of four overlapping peaks at 190, 230, 320 and 530 °C (Figure 6B). The peak at 190 °C could be assigned to the reduction of copper cations ($Cu^{2+} \rightarrow Cu^0$) in oligomeric copper oxide species and small CuO crystallites [30], while the maximum at 230 °C is possibly related to the reduction of monomeric Cu^{2+} cations to Cu^+ ions [31]. The peak at 320 °C could be assigned to two overlapping processes—reduction of Mn^{3+} cations to Mn^{2+} in highly dispersed species [32] and reduction of monomeric Cu^{2+} cations to Cu^+ [31]. Reduction of Mn^{3+} to Mn^{2+} cations in aggregated metal oxide species is possibly represented by a peak at 530 °C [32,36]. However, the reduction of strongly stabilized copper species at higher temperatures cannot be ex-

cluded. The differences in the profile of the bimetallic CuMn sample and cumulative profile of the monometallic (Cu+Mn) samples (Figure 6B), indicate the formation of easy-reducible copper species (reduction below 200 °C) and increased contribution of monomeric copper cations in the CuMn sample in comparison to the Cu sample. Moreover, the obtained results show higher contribution of aggregated manganese species in the bimetallic CuMn sample compared to the monometallic Mn sample.

The reduction profile of the FeMn sample consists of three overlapping peaks at about 260, 460 and 540 °C (Figure 6C). The first peak is possibly related to two overlapping processes—reduction of Fe^{3+} to Fe^{2+} in iron oxide species [32–34] as well as reduction of Mn^{3+} to Mn^{2+} cations in highly dispersed species [36,37]. The main reduction peak at 460 °C and shoulder at about 540 °C are assigned to two overlapping processes—reduction of Mn^{3+} to Mn^{2+} in aggregated metal oxide species [32] and reduction of Fe^{2+} to Fe^{0} in iron oxide species [35]. The profile of the bimetallic FeMn sample and cumulative (Fe+Mn) profile of the monometallic samples are very similar and the main difference is related to various intensities of these profiles. Thus, in contrast to the Cu-containing bimetallic samples, in the case of FeMn, deposited transition metal species and their contribution in bimetallic and monometallic samples are very similar.

Surface acidity of the samples was studied by the NH_3-TPD method. Ammonia desorption profiles are presented in Figure 7, while surface concentration (C_a) and density (D_a) of acid sites in the samples are compared in Table 1. S-MCM-41 non-modified with transition metals do not exhibit any surface acidity (results not shown), thus acid sites are generated by transition metals deposition. Ammonia desorption profiles recorded for the monometallic samples contain two overlapping maxima (Figure 7A). The first, representing ammonia bounded to weaker acid sites, is centred, depending on deposited transition metal, in the range of 140–155 °C. The second broad maximum, assigned to ammonia molecules bounded to stronger acid sites is centred at about 260–280 °C. The shape of the ammonia desorption profiles recorded for monometallic samples based on mesoporous spherical silica of MCM-41 type is very similar to those reported in scientific literature [12,37,38]. Our previous studies [11] showed that deposition of copper and manganese to cylindrical MCM-41 resulted exclusively in Lewis acid sites, while in the case of iron deposition the presence of a small amount of Brønsted type acid sites was also identified. Therefore, the formation of mainly donor–acceptor bonds (coordination bounds) between ammonia molecules (donor of electron pair) and transition metal cations (acceptor of electron pair) is expected in these studies.

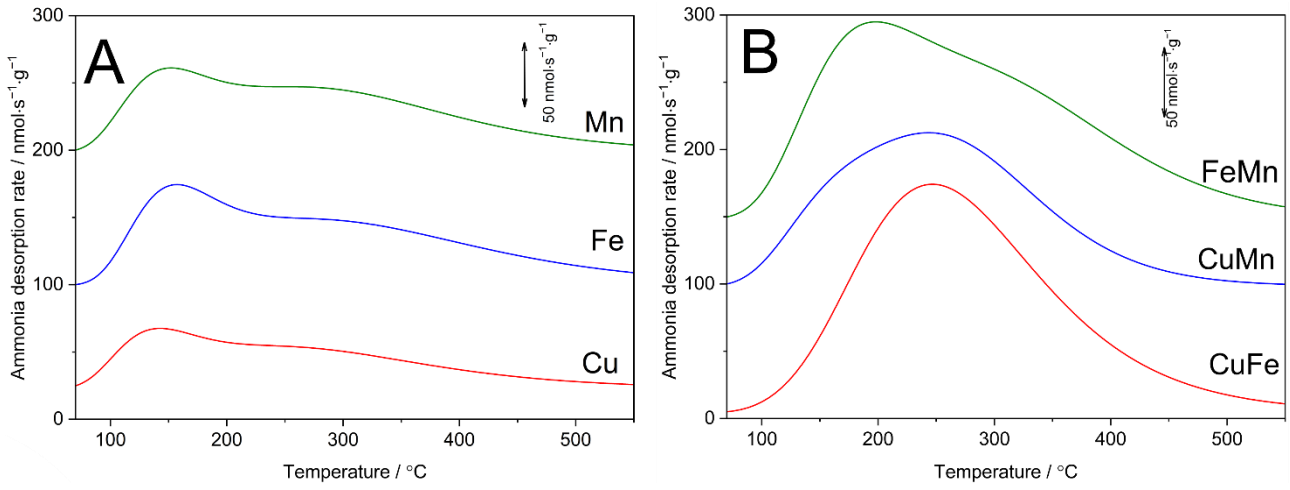

Figure 7. NH_3-TPD profiles of the S-MCM-41 samples monometallic (**A**) and bimetallic systems (**B**).

Ammonia desorption profiles of the bimetallic samples (Figure 7B) are different from the profiles recorded for the monometallic samples (Figure 7A). Desorption profile of the CuFe sample consists of a maximum centred at about 250 °C with a shoulder at higher

temperatures. In the case of the CuMn sample desorption profile is represented by a broad maximum centred at about 245 °C, which is a superposition of at least two peaks. Ammonia desorption profile of the FeMn sample consists of at least two overlapping maxima centred at about 200 and 315 °C. Thus, in the case of the bimetallic samples, the ammonia desorption profiles are not a simple cumulation of desorption profiles of the monometallic samples but represent different distribution of acid sites with respect to their acid strength.

The concentration and density of acid sites in the bimetallic samples are higher than in monometallic samples (Table 1). This is related to higher transition metal loading in the samples modified with pairs of transition metals. The concentration and density of acid sites depend on the transition metal loading and aggregation of deposited metal species. The Cu sample presents the lowest surface concentration of acid sites in a series of the monometallic samples. This is not surprising considering the presence of CuO crystallites in this sample.

S-MCM-41 modified with transition metal species were tested as catalysts of the selective catalytic reduction of NO with ammonia (NH_3-SCR). Results of the catalytic studies for the monometallic Cu and Fe samples, as well as mechanical mixture of monometallic samples (Cu+Fe) and bimetallic CuFe catalyst, are compared in Figure 8A. Monometallic Cu catalyst is active in NO conversion at temperatures above 200 °C, however at higher temperatures the efficiency of the NH_3-SCR process is significantly limited by the side process of direct ammonia oxidation with oxygen present in the reaction mixture. In the case of the Fe catalyst, the NO conversion is observed from about 150 °C and is higher than the conversion obtained for the Cu catalyst in the studied temperature range. Mechanical mixture of monometallic samples (Cu+Fe) presented significantly higher catalytic activity than monometallic catalysts, however the side rection of direct ammonia oxidation decreased the efficiency of the NH_3-SCR process at temperatures above 325 °C. Bimetallic CuFe catalyst presented better catalytic activity than the monometallic samples but was less active than the mechanical mixture of the monometallic catalysts (Cu+Fe). It should be noted that the side process of direct ammonia oxidation was significantly reduced in the case of bimetallic CuFe catalyst in comparison to the mechanical mixture of monometallic catalysts. N_2 and N_2O were the only identified nitrogen-containing products of the NH_3-SCR process. The selectivity to nitrogen, determined for this series of catalysts, is high and did not drop below 90% in the studied temperature range (Figure 8A). The selectivity to nitrogen was on the level of 98–100% in the case of the Fe and CuFe catalysts, while for the Cu sample and mechanical mixture of monometallic (Cu+Fe) samples was in the range of 91–97% at temperatures below 425 °C.

The monometallic Mn catalyst presented lower activity in the NO conversion than the Cu sample at temperatures below 375 °C, however at higher temperatures the efficiency of this catalyst in NH_3-SCR is higher due to its limited activity in the side process of direct ammonia oxidation (Figure 8B). The NO conversion profile of the mechanical mixture of the monometallic (Cu+Mn) catalysts is very similar to the sum of the profiles obtained for the monometallic samples. However, bimetallic CuMn catalyst presented much better activity in the NO conversion than mechanical mixture (Cu+Mn) of the monometallic samples. In this case, the NO conversion started at about 150 °C and the level of the NO conversion above 95% was obtained in the range of 275–325 °C, while at higher temperatures the efficiency of the NH_3-SCR process decreased due to the side process of direct ammonia oxidation. The selectivity to nitrogen of the CuMn catalyst is very close to 100% in the studied temperature range and is higher than for the mechanical mixture (Cu+Mn) of the monometallic samples. It should be noted that the content of copper and manganese is the same in the CuMn catalyst and mechanical mixture of the samples (Cu+Mn) (Table 1). Thus, the simultaneous presence of both copper and manganese species results in the synergistic catalytic effect.

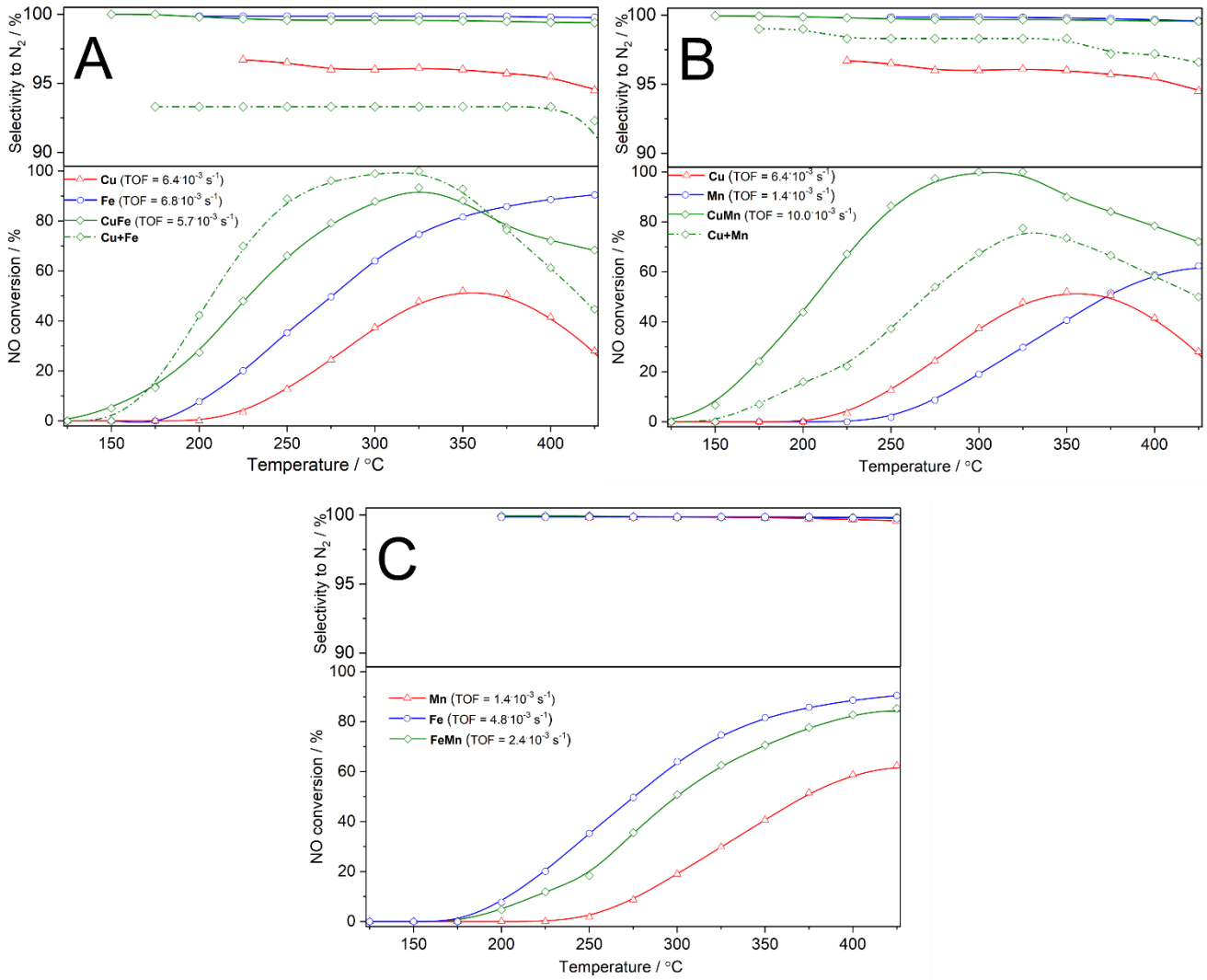

Figure 8. Temperature dependence of NO conversion and N_2 selectivity in SCR with NH_3 for the spherical MCM-41 material modified with Cu-Fe (**A**), Cu-Mn (**B**) and Fe-Mn (**C**) by TIE method; dash-dot line corresponds to mixed monometallic samples.

Catalytic activity of the bimetallic FeMn sample is higher than monometallic Cu catalyst and lower than the Fe sample (Figure 8C). Thus, the simultaneous presence of iron and copper in the catalyst results in decreased catalytic activity in comparison with the monometallic Fe catalyst. Selectivity of the bimetallic FeMn catalyst to nitrogen is close to 100% in the studied temperature range.

The turn-over-frequency (TOF) values determined for the reaction at 275 °C are shown in Figure 8. Because most of the postulated mechanisms of the NH_3-SCR reaction include chemisorption and activation of ammonia molecules as one of the main reaction steps [39], it was therefore assumed that each of the acid sites, determined by the NH_3-TPD method (Figure 7, Table 1), are active sites of the studied reaction. The TOF value determined for the CuMn is much higher than for other catalysts. Moreover, this value (10.0×10^{-3} s^{-1}) is higher than the sum of TOF values determined for the monometallic Cu and Mn samples (7.8×10^{-3} s^{-1}). Thus, this proves the cooperative synergistic effect of copper and manganese in the NH_3-SCR reaction.

Thus, simultaneous presence of both copper and manganese species results in a cooperative synergistic catalytic effect of these metals, which is possibly related to the electron transfers: $Cu^{2+} + Mn^{3+} \rightarrow Cu^{+} + Mn^{4+}$ and $Cu^{2+} + Mn^{2+} \rightarrow Cu^{0} + Mn^{4+}$. Wu et al. [40] have recently reported a significant role of Cu^{2+}/Cu^{+} coexistence in the NH_3-SCR process.

Cu^{2+} cations are adsorption sites of NH_3 and possibly also NO molecules and promote the formation of NO^+ active species as well as dehydrogenation of ammonia molecules. On the other side, Cu^+ can act as the adsorption site for oxygen, promoting the formation of active oxygen O^- species. A similar role was also recently postulated for Cu^0 species by Liu et al. [41]. Thus, the synergistic effect between Cu^{2+} and Cu^+/Cu^0 can result in the rapid formation of reactive intermediates of the NH_3-SCR process. On the other side Mn^{4+} was reported to be active in the dehydrogenation of adsorbed ammonia molecules into reactive -NH_2 intermediate [42] as well as oxygen adsorption with the formation of active oxygen O^- species necessary for activation of the reactants in the NH_3-SCR process. Thus, such active oxygen species can also be reactive in the oxidation of NO to NO_2, which is necessary for the low-temperature nitrogen oxides conversion by fast SCR process, $2NH_3 + NO + NO_2 \rightarrow 2N_2 + 3H_2O$. To verify the activity of the most active bimetallic CuMn catalyst, as well as monometallic Cu and Mn catalysts, additional experiments of NO to NO_2 oxidation were undertaken (Figure 9). As can be seen, the NO to NO_2 oxidation is much more effective in the case of bimetallic CuMn catalyst than for monometallic Cu and Mn catalysts. The estimated NO conversion in the maximum (390 °C) of the CuMn profile is about 50%. The maxima in the profiles of the monometallic samples are shifted into higher temperatures, 400 and 440 °C for the Cu and Mn samples, respectively. Moreover, the estimated NO conversions for these maxima are about 34 and 19% for the Cu and Mn catalysts, respectively. In general, these results are in line with the results of the NH_3-SCR catalytic studies (Figure 8B). The CuMn catalyst presented the highest activity, and the maximum of the NO conversion is at a lower temperature than for the monometallic Cu and Mn samples. Thus, it is postulated that oxidation of NO to NO_2, and therefore the fast SCR pathway, plays an important role in the NO conversion over studied catalysts, especially in the case of bimetallic CuMn catalyst.

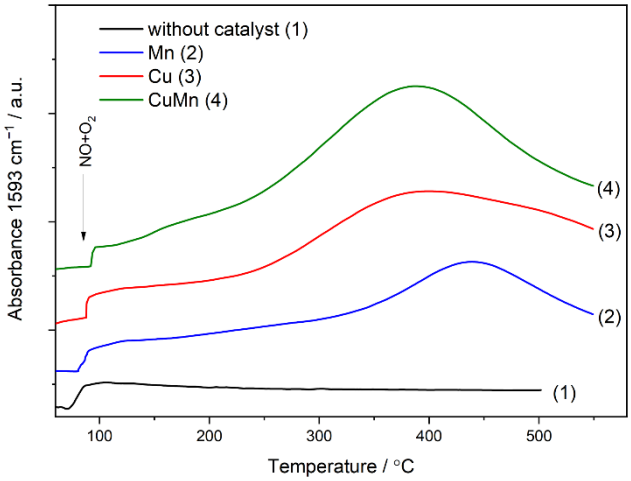

Figure 9. Results of NO to NO_2 oxidation for the reaction without catalyst (1) and for Mn (2), Cu (3) and CuMn (4) samples.

For the most active catalyst, CuMn, additional stability tests were done at 275 °C (Figure 10). In the long-term stability test (Figure 10A), the NO conversion decreased from 96 to 87% during the first 12 h of the stability test and was then stable or even slightly increased. Selectivity to nitrogen was on the level of 99% during 17 h of the stability test. In the second stability test the influence of water vapour presence in the reaction mixture on the catalytic efficiency of NH3-SCR was studied (Figure 10B). In this case water vapour (5 vol.%) was periodically added into the reaction mixture. After 60 min of the test, water vapour was introduced into the rection mixture and the NO conversion decreased from about 97 to 88%. After another 60 min, the water vapour flow was stopped and this resulted in an increase in the NO conversion to about 94%. After the following cycles with wet and dry reaction mixture the NO conversion level of 90% was obtained. The obtained results

indicate that the presence of water vapour in the reaction mixture decreased efficiency of the NH3-SCR process, however deactivation of the catalysts is rather limited and partially reversible after removal of water vapour from the reaction mixture.

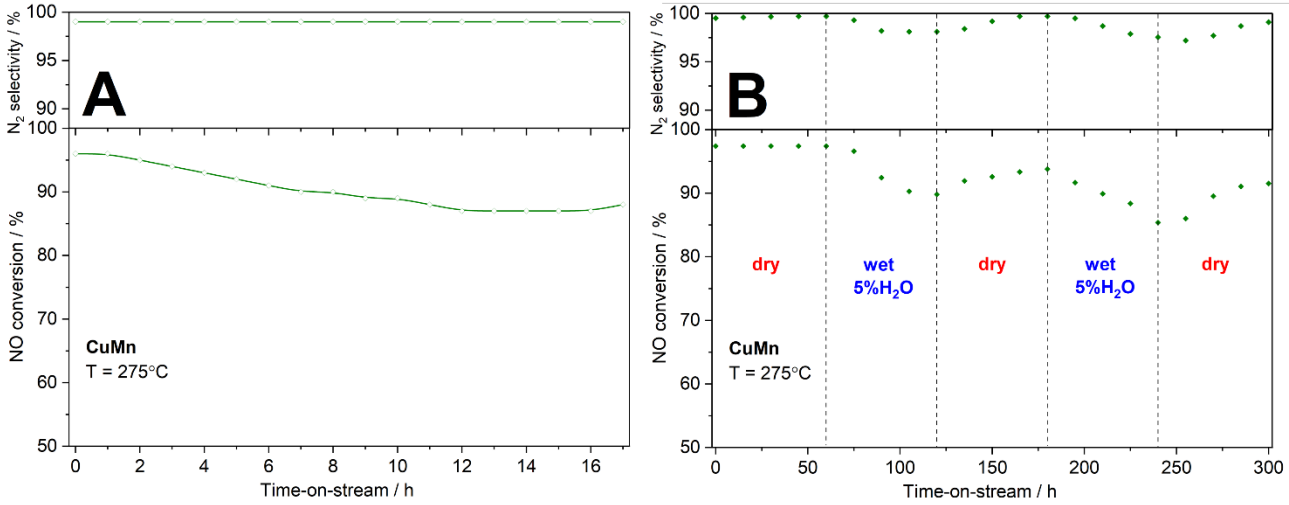

Figure 10. Catalytic stability NH_3-SCR test over the CuMn catalyst at 275 °C for 17 h (**A**) and with periodical exchanges from dry to wet (5 vol.% H_2O) reaction conditions at 275 °C (**B**).

3. Materials and Methods

3.1. Catalyst's Preparation

3.1.1. Synthesis of Spherical MCM-41

The detailed procedure used for the preparation of spherical MCM-41 material has been presented by Liu et al. [43]. According to this procedure, the synthesis of mesoporous silica started from dissolution of organic surfactant, cetyltrimethylammonium bromide (C_{16}TAB, Sigma-Aldrich, St. Louis, MO, USA), in the mixture composed of water (H_2O), ethanol (EtOH, Chempur, Karlsruhe, Germany) and aqueous ammonia ($NH_3 \cdot H_2O$, Avantor/POCH, Gliwice, Poland). The obtained solution was stirred on magnetic stirrer for 15 min at room temperature (RT). Then, tetraethyl orthosilicate (TEOS, Sigma-Aldrich, St. Louis, MO, USA), used as a silica source, was added to the reaction mixture resulting in the synthesis slurry with the following molar ratio of the reactants: 1 TEOS: 0.3 C_{16}TAB: 11 NH_3:58 EtOH: 144 H_2O. The obtained synthesis gel was stirred at RT for the next 2 h and then the obtained solid product was collected by filtration, washed with distilled water, and dried overnight at 60 °C. The dried but non-calcined sample, containing surfactants inside pores, is named as pre-S-MCM-41, while the template-free product, S-MCM-41, was obtained by calcination of the pre-S-MCM-41 sample at 550 °C (a heating rate of 1 °C·min^{-1}) for 6 h in the air atmosphere.

3.1.2. Functionalization of Mesoporous Silica

Pre-S-MCM-41 was modified with transition metals (TM) by the template-ion exchange method (TIE). Mesoporous silica was modified with copper, iron, or manganese as well as pairs of these metals (copper-iron, copper-manganese, iron-manganese). The chlorides of these metals were used as precursors—$CuCl_2$ (POCH, Gliwice, Poland), $FeCl_2$ (Sigma-Aldrich, St. Louis, MO, USA), $MnCl_2$ (Sigma-Aldrich, St. Louis, MO, USA)—while methanol (MeOH, VWR, RadnorPA, PA, USA) was used as a solvent. Pre-S-MCM-41 was introduced into methanolic solution of transition metal chlorides (mono- or bimetallic systems) and intensively stirred at 70 °C for 3 h under reflux. Then, the samples were separated by filtration, washed with pure methanol, and dried overnight at 60 °C. Finally, the obtained materials were calcined in air atmosphere at 550 °C (a heating rate of 1 °C·min^{-1}) for 6 h in the air atmosphere. All samples' codes, as well as details of their modification procedures, are presented in Table 2.

Table 2. The sample codes and amounts of reactants used for TIE method.

Sample Code	Weight of [1] pre-S-MCM-41/g	Solution Volume/cm^3	$CuCl_2 \cdot 2H_2O$ Concentration/mmol	$FeCl_2 \cdot 4H_2O$ Concentration/mmol	$MnCl_2 \cdot 2H_2O$ Concentration/mmol
[2] S-MCM-41	-	-	-	-	-
Cu	2.7	135	0.465	-	-
Fe	2.7	135	-	0.465	-
Mn	2.7	135	-	-	0.465
CuFe	2.7	135	0.465	0.465	-
CuMn	2.7	135	0.465	-	0.465
FeMn	2.7	135	-	0.465	0.465

[1] Non-calcined spherical MCM-41. [2] Calcined spherical MCM-41.

3.2. Catalyst's Characterization

The morphology of the samples was examined by scanning electron microscope analysis (SEM). SEM micrographs were collected by using a Hitachi S-4700 scanning electron microscope (Hitachi Instruments Inc., San Jose, CA, USA) equipped with a Noran Vantage analyser.

The powder X-ray diffraction patterns of the spherical mesoporous silica and its modifications with transition metals were obtained with a Bruker D2 Phaser diffractometer (Bruker, Billerica, MA, USA). The measurements were conducted in the range of low 2θ angle (1–8°) and in the high 2θ angle (28–42°) with 2θ step scans of 0.02° with a counting time of 5 s and 2 s per step, respectively.

Inductively coupled plasma optical emission spectrometry (iCAP 7400, Thermo Scientific, Waltham, MA, USA) was used for the determination of the chemical composition (Si, Cu, Fe, Mn) of the transition metals modified silica samples. The solid samples were dissolved in a mixture of 6 mL HNO_3 (67–69%, Honeywell, Charlotte, NC, USA), 2 mL HCl (30%, Honeywell, Charlotte, NC, USA), and 2 mL HF (47–51%, Honeywell, Charlotte, NC, USA) at 190 °C using a microwave digestion system (Ethos Easy, Milestone, Sorisole, Italy).

The porosity of the samples was determined by low-temperature N_2 sorption at −196 °C using a 3Flex (Micromeritics, Norcross, GA, USA) automated gas adsorption system. Before the analysis, the samples were degassed under vacuum at 350 °C for 24 h. The specific surface area (S_{BET}) of the samples was determined by application of the BET equation. The pore size distributions were determined from the adsorption branch of nitrogen isotherm by applying the BJH model method, while the pore volume was calculated using the total amount of nitrogen adsorbed at $p/p_0 = 0.98$.

UV-Vis DR spectra were recorded in the range of 200–800 nm with a resolution of 2 nm using spectrophotometer Lambda 650 S (Perkin Elmer, Waltham, MA, USA).

Temperature-programmed desorption of ammonia (NH_3-TPD) was applied for analysis of the surface acidity of the samples. Prior to the NH_3-TPD run, the sample (50 mg), placed in a fixed-bed quartz microreactor, was outgassed at 550 °C for 30 min. Then, the microreactor with the sample was cooled to 70 °C and saturated in a flow of gas mixture containing 1 vol.% NH_3 diluted in He (flow rate of 20 mL·min^{-1}) followed by flushing with pure helium to remove ammonia physisorbed on the sample surface. Finally, the temperature-programmed desorption of ammonia was carried out with a linear heating rate of 10 °C·min^{-1} in a flow of pure helium (20 mL·min^{-1}). All experimental stages of NH_3-TPD were monitored by a quadrupole mass spectrometer—QMS (PREVAC, Rogów, Poland) connected directly to the microreactor outlet. Recalculation of the detector signal into the ammonia desorption rate was based on the calibration of the QMS with commercial gas mixtures.

Temperature-programmed reduction with H_2 (H_2-TPR) was used to analyse the reducibility of the transition metal species deposited on silica supports. The experiment was carried out in a fixed-bed flow microreactor system appointed with a thermal conductivity detector—TCD (Valco, Houston, TX, USA). Prior to each H_2-TPR experiment, 50 mg of the sample was placed in the reactor and degassed in a flow of pure Ar at 550 °C for

20 min. Subsequently, the system was cooled to 80 °C and the temperature-programmed reduction process was started. In the H_2-TPR process, the catalyst was reduced in a flow of 5 vol.% H_2/Ar (10 mL·min^{-1}) in the temperature range of 80–725 °C with a linear heating of 10 °C·min^{-1}.

3.3. Catalytic Studies

3.3.1. NH_3-SCR

The catalysts were tested in the process of the selective catalytic reduction of NO with ammonia (NH_3-SCR). Catalytic studies were performed in the experimental system consisting of a fixed-bed quartz microreactor with the outlet connected directly to the detector—quadrupole mass spectrometer—QMS (PREVAC, Rogów, Poland). The used gas mixture contained 0.25 vol.% NO, 0.25 vol.% NH_3 and 2.5 vol.% O_2 diluted in pure He (total flow rate of 40 mL·min^{-1}). Before the catalytic test, 100 mg of the sample (particle size in the range of 250–315 μm) was placed in a quartz microreactor and outgassed in the flow of He at 550 °C for 30 min. After the microreactor cooled to 100 °C, the catalytic test was initiated with a linear heating rate of 10 °C·min^{-1}, in the temperature range of 100–425 °C. Catalytic tests were performed under atmospheric pressure.

Moreover, the catalytic tests of NH_3-SCR for mechanical mixtures of monometallic catalysts were done. For each experiment, 100 mg of two monometallic samples were mixed resulting in 200 mg of catalyst placed in the microreactor space. The particles size, degassing procedure, reaction conditions and catalytic-detection system were the same as those described earlier.

For the most active catalyst, CuMn, isothermal long-term stability NH_3-SCR and stability isothermal NH_3-SCR test with periodical exchange from dry to wet reaction mixtures were done. Both experiments were conducted at 275 °C. The composition of the reaction mixture was the same as in polythermic catalytic tests. In the case of the test in wet conditions 5 vol% of water vapour was introduced into the reaction mixture.

3.3.2. NO to NO_2 Oxidation Process

The studies of catalytic NO to NO_2 oxidation were carried out in the same system as the NH_3-SCR tests. The only difference was using an FTIR detector instead of a QMS analyser. The reaction was studied in a flow of gas mixture containing 0.5 vol.% NO and 2.5 vol.% O_2 diluted in He (total flow rate of 40 mL min^{-1}). FTIR spectrometer Nicolet iS5 (Thermo Scientific, Waltham, MA, USA), equipped with a gas cell of 10 cm length, operating in the wavenumber range of 625–4000 cm^{-1} and with a resolution of 4 cm^{-1}, was used for the analysis of the reaction mixture down-stream as well as up-stream of the microreactor. The bands at 1593 and 1912 cm^{-1} were used for the analysis of NO_2 and NO, respectively.

4. Conclusions

Spherical MCM-41 samples, modified with copper, iron, or manganese as well as pairs of these transition metals by the TIE method, were studied in their role as NH_3-SCR catalysts. In the case of monometallic catalysts, the TIE method resulted in the deposition of iron and manganese in the form of highly dispersed metal species, while in the samples modified with copper, besides highly dispersed forms of this metal, small crystallites of CuO also appeared. The formation of such CuO crystallites was significantly limited in the case of bimetallic copper-iron sample and was not observed in the copper-manganese catalyst. The reducibility of the bimetallic catalysts was significantly modified in relation to the reducibility of the monometallic samples. In the case of bimetallic copper-containing samples this effect was assigned to the better dispersion of this metal compared to monometallic copper catalyst. Also, surface acidity, analysed by the NH_3-TPD method, was significantly modified in the case of the bimetallic samples. The main maximum in ammonia desorption profiles of the bimetallic samples was shifted to higher temperatures, indicating increased contribution of stronger acid sites in these samples in comparison to the monometallic catalysts. Catalytic activity of bimetallic copper-iron and copper-manganese catalysts in

the NH_3-SCR process was significantly better than corresponding monometallic catalysts. Moreover, in the case of the bimetallic copper-manganese catalyst the efficiency of the NH_3-SCR reaction was significantly higher than for the mechanical mixture of monometallic copper and manganese catalysts in the studied temperature range. Also, the selectivity to nitrogen was significantly higher for bimetallic catalyst than for the mixture of the monometallic catalysts. The synergistic effect of copper and manganese is possibly related to the electron transfers: $Cu^{2+} + Mn^{3+} \rightarrow Cu^{+} + Mn^{4+}$ and $Cu^{2+} + Mn^{2+} \rightarrow Cu^{0} + Mn^{4+}$. Such Cu^{+} cations probably act as oxygen adsorption sites, promoting the formation of oxygen O^{-} species active in the formation of reactive intermediates of the NH_3-SCR process. Furthermore, Mn^{4+} cations are active in dehydrogenation of adsorbed ammonia molecules into reactive -NH_2 intermediate as well as oxygen adsorption with the formation of reactive oxygen O^{-} species. Such oxygen species, formed in the presence of Cu^{+} and Mn^{4+}, are supposed to intensify the efficiency of NO to NO_2 oxidation. The increased activity of bimetallic CuMn in comparison to the mechanical mixture of monometallic catalysts (Cu+Mn) in the reaction of NO to NO_2 oxidation was experimentally proved. NO_2 formed in this reaction is necessary for the low-temperature nitrogen oxides conversion by fast SCR process, which is one of the main reaction pathways of the low-temperature NOx conversion. Thus, the fast SCR reaction seems to be an important pathway of nitrogen oxide conversion over bimetallic CuMn catalyst. The copper-manganese catalyst presented high stability in the long-term isothermal catalytic test in dry and wet conditions. Thus, it could be concluded that copper-manganese catalyst based on spherical MCM-41 is promising for the low-temperature NH_3-SCR process.

Supplementary Materials: The following supporting information can be downloaded at: https://www.mdpi.com/article/10.3390/catal12080885/s1, Figure S1: Scanning electron micrographs of spherical MCM-41 particles; Figure S2: SEM images of the spherical MCM-41 samples modified by TIE method with Cu (A), Fe (B), Mn (C); Figure S3: SEM images of the spherical MCM-41 samples modified by TIE method with CuFe (A), CuMn (B), FeMn (C); Figure S4: N_2 adsorption-desorption isotherms of the spherical MCM-41 samples modified by TIE method with Cu, Fe, Mn (A) and their bimetallic systems (B).

Author Contributions: Conceptualization, A.J. and L.C.; methodology, A.J. and L.C.; investigation, A.J., A.K., M.R. and M.M.; data curation, A.J. and L.C.; writing—original draft preparation, A.J. and L.C.; writing—review and editing, A.J and L.C.; visualization, A.J. and L.C.; supervision, L.C.; project administration, L.C. All authors have read and agreed to the published version of the manuscript.

Funding: This research was funded by the National Science Centre (Poland), grant number 2018/31/B/ST5/00143. A.J. has been partly supported by the EU Project POWR.03.02.00-00-I004/16.

Data Availability Statement: Experimental data are available from the authors on the request.

Acknowledgments: The studies were carried out in the frame of project 2018/31/B/ST5/00143 from the National Science Centre (Poland).

Conflicts of Interest: The authors declare no conflict of interest.

References

1. Cohn, J.G.; Steele, D.R.; Andersen, H.C. Method of Selectively Removing Oxides of Nitrogen from Oxygen-Containing Gases. U.S. Patent US2975025, 14 March 1961.
2. Surhone, L.M.; Timpledon, M.T.; Marseken, S.F. *Selective Catalytic Reduction*; Betascript Publishing: Beau Bassin, Mauritius, 2010.
3. Marberger, A.; Elsener, M.; Ferri, D.; Kröcher, O. VO_x Surface Coverage Optimization of V_2O_5/WO_3-TiO_2 SCR Catalysts by Variation of the V Loading and by Aging. *Catalysts* **2015**, *5*, 1704–1720. [CrossRef]
4. Chmielarz, L.; Jankowska, A. Mesoporous silica-based catalysts for selective catalytic reduction advances—Recent advances. In *Advances in Inorganic Chemistry: Recent Highlights II*; van Eldik, R., Hubbard, C.D., Eds.; Academic Press: Cambridge, MA, USA, 2022; Volume 79, pp. 205–241.
5. Beale, A.M.; Gao, F.; Lezcano-Gonzalez, I.; Peden, C.H.F.; Szanyi, J. Recent advances in automotive catalysis for NO_x emission control by small-pore microporous materials. *Chem. Soc. Rev.* **2015**, *44*, 7371–7405. [CrossRef]
6. Shan, Y.L.; Du, J.P.; Zhang, Y.; Shan, W.P.; Shi, X.Y.; Yu, Y.B.; Zhang, R.D.; Meng, X.J.; Xiao, F.S.; He, H. Selective catalytic reduction of NO_x with NH_3: Opportunities and challenges of Cu-based small-pore zeolites. *Natl. Sci. Rev.* **2021**, *8*, nwab010. [CrossRef]

7. Chmielarz, L.; Dziembaj, R. Modified Layered Silicas as Catalysts for Conversion of Nitrogen Pollutants in Flue Gases—A Review. *Catalysts* **2021**, *11*, 644. [CrossRef]
8. Jankowska, A.; Chłopek, A.; Kowalczyk, A.; Rutkowska, M.; Mozgawa, W.; Michalik, M.; Liu, S.; Chmielarz, L. Enhanced catalytic performance in low-temperature NH_3-SCR process of spherical MCM-41 modified with Cu by template ion-exchange and ammonia treatment. *Microporous Mesoporous Mater.* **2021**, *315*, 110920. [CrossRef]
9. Jankowska, A.; Chłopek, A.; Kowalczyk, A.; Rutkowska, M.; Michalik, M.; Liu, S.; Chmielarz, L. Catalytic Performance of Spherical MCM-41 Modified with Copper and Iron as Catalysts of NH_3-SCR Process. *Molecules* **2020**, *25*, 5651. [CrossRef] [PubMed]
10. Kowalczyk, A.; Święs, A.; Gil, B.; Rutkowska, M.; Piwowarska, Z.; Borcuch, A.; Michalik, M.; Chmielarz, L. Effective catalysts for the low-temperature NH_3-SCR process based on MCM-41 modified with copper by template ion-exchange (TIE) method. *Appl. Catal. B Environ.* **2018**, *237*, 927–937. [CrossRef]
11. Kowalczyk, A.; Borcuch, A.; Michalik, M.; Rutkowska, M.; Gil, B.; Sojka, Z.; Indyka, P.; Chmielarz, L. MCM-41 modified with transition metals by template ion-exchange method as catalysts for selective catalytic oxidation of ammonia to dinitrogen. *Microporous Mesoporous Mater.* **2017**, *240*, 9–21. [CrossRef]
12. Jankowska, A.; Kowalczyk, A.; Rutkowska, M.; Michalik, M.; Chmielarz, L. Spherical Al-MCM-41 Doped with Copper by Modified TIE Method as Effective Catalyst for Low-Temperature NH_3-SCR. *Molecules* **2021**, *26*, 1807. [CrossRef] [PubMed]
13. Zhang, N.; Li, L.; Guo, Y.; He, J.; Wu, R.; Song, L.; Zhang, G.; Zhao, J.; Wang, D.; He, H. A MnO_2-based catalyst with H_2O Resistance for NH_3-SCR: Study of Catalytic Activity and Reactants-H_2O Competitive Adsorption. *Appl. Catal. B Environ.* **2020**, *270*, 118860. [CrossRef]
14. Fang, X.; Liu, Y.; Cheng, Y.; Cen, W. Mechanism of Ce-Modified Birnessite-MnO_2 in Promoting SO_2 Poisoning Resistance for Low-Temperature NH_3-SCR. *ACS Catal.* **2021**, *11*, 4125–4135. [CrossRef]
15. Yang, G.; Zhao, H.; Luo, X.; Shi, K.; Zhao, H.; Wang, W.; Chen, Q.; Fan, H.; Wu, T. Promotion effect and mechanism of the addition of Mo on the enhanced low temperature SCR of NO_x by NH_3 over MnO_x/γ-Al_2O_3 catalysts. *Appl. Catal. B Environ.* **2019**, *245*, 743–752. [CrossRef]
16. Lu, X.; Song, C.; Jia, S.; Tong, Z.; Tang, X.; Teng, Y. Low-temperature selective catalytic reduction of NO_x with NH_3 over cerium and manganese oxides supported on TiO_2–graphene. *Chem. Eng. J.* **2015**, *260*, 776–784. [CrossRef]
17. Chen, Q.-L.; Guo, R.-T.; Wang, Q.-S.; Pan, W.-G.; Wang, W.-H.; Yang, N.-Z.; Lu, C.-Z.; Wang, S.-X. The catalytic performance of Mn/$TiWO_x$ catalyst for selective catalytic reduction of NO_x with NH_3. *Fuel* **2016**, *181*, 852–858. [CrossRef]
18. Li, J.; Guo, J.; Shi, X.; Wen, X.; Chu, Y.; Yuan, S. Effect of aluminum on the catalytic performance and reaction mechanism of Mn/MCM-41 for NH_3-SCR reaction. *Appl. Surf. Sci.* **2020**, *534*, 147592. [CrossRef]
19. Hung, N.H.; Thanh, N.D.; Lam, N.H.; Dien, N.D.; Chien, N.D.; Vuong, D.D. Preparation and ethanol sensing properties of flower-like cupric oxide hierarchical nanorods. *Mater. Sci. Semicond. Process.* **2014**, *26*, 18–24. [CrossRef]
20. Kowalczyk, A.; Piwowarska, Z.; Macina, D.; Kuśtrowski, P.; Rokicińska, A.; Michalik, M.; Chmielarz, L. MCM-41 modified with iron by template ion-exchange method as effective catalyst for DeNOx and NH_3-SCO processes. *Chem. Eng. J.* **2016**, *295*, 167–180. [CrossRef]
21. Leofanti, G.; Padovan, M.; Tozzola, G.; Venturelli, B. Surface area and pore texture of catalysts. *Catal. Today* **1998**, *41*, 207–219. [CrossRef]
22. Thommes, M.; Kaneko, K.; Neimark, A.V.; Olivier, J.P.; Rodriguez-Reinoso, F.; Rouquerol, J.; Sing, K.S.W. Physisorption of gases, with special reference to the evaluation of surface area and pore size distribution (IUPAC Technical Report). *Pure Appl. Chem.* **2015**, *87*, 1051–1069. [CrossRef]
23. Martins, L.; Peguin, R.P.S.; Wallau, M.; Urquieta, G. Cu-, Co-, Cu/Ca- and Co/Ca-exchanged ZSM-5 zeolites: Activity in the reduction of NO with methane or propane. *Stud. Surf. Sci. Catal.* **2004**, *154*, 2475–2483.
24. Rutkowska, M.; Piwowarska, Z.; Micek, E.; Chmielarz, L. Hierarchical Fe-, Cu- and Co-Beta zeolites obtained by mesotemplate-free method. Part I: Synthesis and catalytic activity in N_2O decomposition. *Microporous Mesoporous Mater.* **2015**, *209*, 54–65. [CrossRef]
25. Kumar, M.S.; Schwidder, M.; Grünert, W.; Brückner, A. On the nature of different iron sites and their catalytic role in Fe-ZSM-5 $DeNO_x$ catalysts: New insights by a combined EPR and UV/VIS spectroscopic approach. *J. Catal.* **2004**, *227*, 384–397. [CrossRef]
26. Kumar, M.S.; Perez-Ramirez, J.; Debbagh, M.N.; Smarsly, B.; Bentrup, U.; Brückner, A. Evidence of the vital role of the pore network on various catalytic conversions of N_2O over Fe-silicalite and Fe-SBA-15 with the same iron constitution. *Appl. Catal. B Environ.* **2006**, *62*, 244–254. [CrossRef]
27. Wójtowicz, M.A.; Pels, J.R.; Moulijn, J.A. Combustion of coal as a source of N_2O emission. *Fuel Process. Technol.* **1993**, *34*, 1–71. [CrossRef]
28. Suzuki, E.; Nakashiro, K.; Ono, Y. Hydroxylation of Benzene with Dinitrogen Monoxide over H-ZSM-5 Zeolite. *Chem. Lett.* **1988**, *17*, 953–956. [CrossRef]
29. Ludvikova, J.; Jablonska, M.; Jiratova, K.; Chmielarz, L.; Balabanova, J.; Kovanda, F.; Obalova, L. Co-Mn-Al mixed oxides as catalysts for ammonia oxidation to N_2O. *Res. Chem. Intermed.* **2016**, *42*, 2669–2690. [CrossRef]
30. Basąg, S.; Piwowarska, Z.; Kowalczyk, A.; Węgrzyn, A.; Baran, R.; Gil, B.; Michalik, M.; Chmielarz, L. Cu-Mg-Al hydrotalcite-like materials as precursors of effective catalysts for selective oxidation of ammonia to dinitrogen—The influence of Mg/Al ratio and calcination temperature. *Appl. Clay Sci.* **2016**, *129*, 122–130. [CrossRef]

31. Boroń, P.; Chmielarz, L.; Dźwigaj, S. Influence of Cu on the catalytic activity of Fe-BEA zeolites in SCR of NO with NH_3. *Appl. Catal. B Environ.* **2015**, *168–169*, 377–384. [CrossRef]
32. Zhang, Q.; Li, Y.; An, D.; Wang, Y. Catalytic behavior and kinetic features of FeOx/SBA-15 catalyst for selective oxidation of methane by oxygen. *Appl. Catal. A Gen.* **2009**, *356*, 103–111. [CrossRef]
33. Macina, D.; Piwowarska, Z.; Góra-Marek, K.; Tarach, K.; Rutkowska, M.; Girman, V.; Błachowski, A.; Chmielarz, L. SBA-15 loaded with iron by various methods as catalyst for DeNOx process. *Mater. Res. Bull.* **2016**, *78*, 72–82. [CrossRef]
34. Arena, F.; Gatti, G.; Martra, G.; Coluccia, S.; Stievano, L.; Spadaro, L.; Famulari, P.; Parmaliana, A. Structure and reactivity in the selective oxidation of methane to formaldehyde of low-loaded FeO_x /SiO_2 catalysts. *J. Catal.* **2005**, *231*, 365–380. [CrossRef]
35. Wei, X.; Zhou, Y.; Li, Y.; Shen, W. Polymorphous transformation of rod-shaped iron oxides and their catalytic properties in selective reduction of NO by NH_3. *RSC Adv.* **2015**, *5*, 66141–66146. [CrossRef]
36. Ling, W.; Huiping, Z.; Ying, Y.; Xinya, Z. Total oxidation of isopropanol over manganese oxide modified ZSM-5 zeolite membrane catalysts. *RSC Adv.* **2015**, *5*, 29482–29490. [CrossRef]
37. Yao, X.; Zhang, J.; Liang, X.; Long, C. Niobium doping enhanced catalytic performance of Mn/MCM-41 for toluene degradation in the NTP-catalysis system. *Chemosphere* **2019**, *230*, 479–487. [CrossRef] [PubMed]
38. Jankowska, A.; Ciuba, J.; Kowalczyk, A.; Rutkowska, M.; Piwowarska, Z.; Michalik, M.; Chmielarz, L. Mesoporous silicas of MCM-41 type modified with iron species by template ion-exchange method as catalysts for the high-temperature NH_3-SCR process—Role of iron species aggregation, silica morphology and associated reactions. *Catal. Today* **2022**, *390–391*, 281–294. [CrossRef]
39. Busca, G.; Lietti, L.; Ramis, G.; Berti, F. Chemical and mechanistic aspects of the selective catalytic reduction of NO_x by ammonia over oxide catalysts: A review. *Appl. Catal. B Environ.* **1998**, *18*, 1–36. [CrossRef]
40. Wu, X.; Meng, H.; Du, Y.L.; Liu, J.N.; Hou, B.H.; Xie, X.M. Insight into Cu_2O/CuO collaboration in the selective catalytic reduction of NO with NH_3: Enhanced activity and synergistic mechanism. *J. Catal.* **2020**, *384*, 72–87. [CrossRef]
41. Liu, K.; Yu, Q.; Wang, B.; San, J.; Duan, W.; Qin, Q. Binary copper-manganese based catalysts with urea for low-temperature selective catalytic reduction of NO: Performance, characterization and mechanism. *Appl. Surf. Sci.* **2020**, *508*, 144755. [CrossRef]
42. Xie, S.; Li, L.; Jin, L.; Wu, Y.; Liu, H.; Qin, Q.; Wei, X.; Liu, J.; Dong, L.; Li, B. Low temperature high activity of M (M = Ce, Fe, Co, Ni) doped M-Mn/TiO_2 catalysts for NH_3-SCR and in situ DRIFTS for investigating the reaction mechanism. *Appl. Surf. Sci.* **2020**, *515*, 146014. [CrossRef]
43. Liu, S.; Lu, L.; Yang, Z.; Cool, P.; Vansant, E.F. Further investigations on the modified Stöber method for spherical MCM-41. *Mater. Chem. Phys.* **2006**, *97*, 203–206. [CrossRef]